Appl. Phys. A 79, 1695–1709 (2004)
DOI: 10.1007/s00339-004-2684-0

Applied Physics A
Materials Science & Processing

S.S. MAO[1,✉]
F. QUÉRÉ[2]
S. GUIZARD[3]
X. MAO[1]
R.E. RUSSO[1]
G. PETITE[3]
P. MARTIN[2]

Dynamics of femtosecond laser interactions with dielectrics

[1] Lawrence Berkeley National Laboratory, University of California, Berkeley, CA 94720, USA
[2] Service des Photons, Atomes et Molécules, CEA/DSM/DRECAM, CEA Saclay, 91191 Gif-sur-Yvette Cedex, France
[3] Laboratoire des Solides Irradiés, CEA/DSM/DRECAM, Ecole Polytechnique, 91128 Palaiseau Cedex, France

Received: 16 October 2003/Accepted: 4 February 2004
Published online: 23 June 2004 •

ABSTRACT Femtosecond laser pulses appear as an emerging and promising tool for processing wide bandgap dielectric materials for a variety of applications. This article aims to provide an overview of recent progress in understanding the fundamental physics of femtosecond laser interactions with dielectrics that may have the potential for innovative materials applications. The focus of the overview is the dynamics of femtosecond laser-excited carriers and the propagation of femtosecond laser pulses inside dielectric materials.

PACS 61.80.Ba; 52.38.Mf; 42.65.Jx; 78.47.+p; 71.35.-y

1 Introduction

Lasers that can produce coherent photon pulses with duration in the femtosecond regime have opened up new frontiers in materials research with extremely short temporal resolution and high photon intensity. The ultrafast feature of femtosecond lasers has been used to observe, in real time, phenomena including chemical reactions in gases [1] or electron-lattice energy transfer in solids [2]. In the meantime, the enormous intensity that femtosecond laser pulses achieve at their focus can create an energetic plasma that emits X-ray photons, which may have potential applications for characterizing microscopic transient structures of materials [3, 4].

The conventional view of pulsed laser-material interactions, with wavelength between near infrared (IR) and near ultraviolet (UV), includes the transfer of electromagnetic energy to electronic excitation, followed by electron-lattice interactions that convert energy into heat. However, the processes of material response following intense femtosecond laser irradiation are far more complex, particularly for wide bandgap dielectrics. When a dielectric material is subject to intense femtosecond laser irradiation, the refractive index of the material may become intensity dependent, and a large amount of excited electrons may be generated by IR pulses in "transparent" dielectrics. Relaxation channels of electronic excitation in wide bandgap materials may produce intrinsic defects, leading to photoinduced damages in the otherwise "defect-free" medium. These fundamentally nonlinear processes have stimulated substantial research efforts in both the understanding of the complexity of femtosecond laser interactions with dielectrics and the applications of the underlying microscopic mechanisms to innovative materials fabrication. This article aims to provide an overview of recent progress in understanding the fundamental physics of femtosecond laser interactions with dielectrics that are important for materials processing applications. Related topics of laser interactions with semiconductors (narrow bandgap materials) have been discussed in several excellent reviews [5, 6].

As a source of energy in a highly concentrated form, lasers in general have become viable tools for material modification since their invention more than four decades ago. The increasing availability of intense femtosecond lasers is fueling a growing interest in high-precision materials processing. In contrast to material modification using nanosecond or longer laser pulses where standard modes of thermal processes dominate, for femtosecond laser-material interactions, only a very small fraction of the laser pulse energy is transmitted as heat and transferred to the material surrounding the laser-irradiated area. Consequently, femtosecond laser pulses can induce nonthermal structural changes, driven directly by electronic excitation and associated nonlinear processes, before the material lattice has equilibrated with the excited carriers. This fast mode of material modification can result in vanishing thermal stress and minimal collateral damage for processing practically any solid-state material. Additionally, damages produced by femtosecond laser pulses are far more regular from shot to shot. These breakdown characteristics make femtosecond lasers ideal tools for precision materials processing.

For femtosecond laser interactions with dielectrics, in addition to their classical value in elucidating the origin of laser-induced breakdown in optical materials, structural modifications of dielectrics are of particular significance to bulk microstructuring that creates subwavelength "voxels". As an example, femtosecond laser pulses can be focused inside transparent dielectric materials in a layer-by-layer fashion. High-density, three-dimensional optical storage was achieved as the result of femtosecond laser-induced submicron structural transition that locally alters the refractive index at the laser pulse's focus [7–10]. Similarly, three-dimensional pho-

✉ Fax: +1-510/486-7303, E-mail: ssmao@lbl.gov

tonic bandgap lattices were realized by spatially organized micropatterning of transparent dielectrics using femtosecond laser pulses [11].

Despite the promise of femtosecond laser pulses in processing wide bandgap dielectric materials for a variety of applications, understanding the fundamental aspects of intense femtosecond laser interactions with dielectrics has been a challenging task. It is the objective of this article to provide an overview of recent efforts at uncovering the subtleties of femtosecond laser interactions with wide bandgap dielectrics, in particular, the ultrafast time-resolved studies of the dynamics of electronic excitation and pulse propagation that are related to material modification.

The remainder of this article is organized as follows. The rest of Sect. 1 offers a short review of individual basic physical processes involved in intense laser interactions with wide bandgap dielectrics. Detailed accounts of some time-resolved experiments on the dynamics of femtosecond laser-induced electronic excitation and relaxation (Sect. 2) and the nonlinear optical processes associated with femtosecond pulse propagation (Sect. 3) are presented in the next two sections. Section 4 is the summary.

1.1 *Carrier excitation*

The problem of carrier excitation and ionization in the case of wide bandgap materials subject to a laser electromagnetic field has been extensively addressed in the literature. The balance between different ionization channels during femtosecond laser interactions with dielectric materials is still under discussion. In the simplest case, the laser can deposit energy into a material by creating electron–hole plasma through single-photon absorption. However, for wide bandgap dielectrics, the cross section of such linear absorption is extremely small. Instead, under intense femtosecond laser irradiation, nonlinear processes such as multiphoton, tunnel, or avalanche ionization become the dominant mechanisms to create free carriers inside the materials.

1.1.1 Photoionization. For irradiation of wide bandgap materials using femtosecond laser pulses with wavelength near the visible (from near IR to near UV), a single laser photon does not have sufficient energy to excite an electron from the valence band to the conduction band. Simultaneous absorption of multiple photons must be involved to excite a valence band electron, with the resulting photoionization rate strongly depending on the laser intensity (Fig. 1a). The rate of multiphoton absorption can be expressed as σI^m, where I is the laser intensity and σ is the cross section of m-photon absorption for a valence band electron to be excited to the conduction band. The number of photons required is determined by the smallest m that satisfies the relation, $m\hbar\omega > E_g$, where E_g is the bandgap energy of the dielectric material and $\hbar\omega$ is the photon energy. We emphasize here one feature of femtosecond laser irradiation: since femtosecond laser pulses offer much higher peak intensities than conventional pulses, they can induce significant intrinsic high-order interband transitions in contrast to the ever-present defect-related processes (of a lower order).

A second photoionization process, tunneling ionization, may come into play during femtosecond laser interactions with dielectrics under an extremely strong laser electromagnetic field, for example, when the laser pulse is very short (e.g., < 10 fs). This process has been extensively investigated in atoms and molecules. In the strong-field regime, the superposition of the nucleus Coulomb field and the laser electric field results in an oscillating finite potential barrier through which bound electrons can tunnel, thus escaping the atom. In dielectrics this mechanism allows the valence electrons to tunnel to the conduction band in a time shorter than the laser period. Both the multiphoton and the tunneling ionization can be treated under the same theoretical framework developed by Keldysh [12]. The transition from multiphoton to tunneling ionization is characterized by the Keldysh parameter [12], $\gamma = \omega \left(2m^* E_g\right)^{1/2} / eE$, where m^* and e are the effective mass and charge of the electron and E is the amplitude of the laser electric field oscillating at frequency ω. When γ is much larger than one, which is the case for most materials-related investigations of laser interactions with dielectrics, multiphoton ionization dominates the excitation process.

1.1.2 Free carrier absorption. An electron being excited to the conduction band of a wide bandgap dielectric material can absorb several laser photons sequentially, moving itself to higher energy states where free carrier absorption is efficient (Fig. 1b). The absorption coefficient α_0, which equals the inverse of the absorption depth, depends on the imaginary part of the refractive index κ, $\alpha_0 = 2\omega\kappa/c$, where c is the speed of light. The complex refraction index, $\tilde{n} = n + i\kappa$, is related to dielectric function $\tilde{\varepsilon}$, which, according to the Drude model [13, 14], can be expressed by

$$\tilde{\varepsilon} = 1 - \omega_p^2 \left[\frac{\tau^2}{1+\omega^2\tau^2} + i \frac{\tau^2}{\omega\tau\left(1+\omega^2\tau^2\right)} \right],$$

with τ the scattering time typically a fraction of a femtosecond depending on the conduction electron energy. For wide bandgap dielectrics under intense laser irradiation, strong

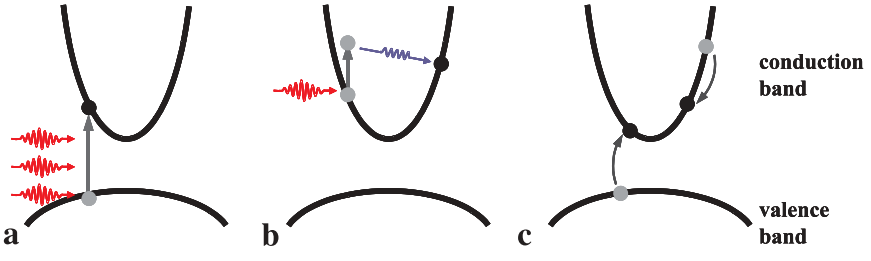

FIGURE 1 Schematic illustration of **a** multiphoton ionization, **b** free carrier absorption, and **c** impact ionization [6]

electron interactions with the lattice are characterized by both the polar and nonpolar phonon scattering [15, 16]. In the expression of $\tilde{\varepsilon}$, ω_p is the plasma frequency defined by

$$\omega_p = \sqrt{\frac{e^2 N}{\varepsilon_0 m^*}} ,$$

where N is the carrier density and ε_0 is the electric permittivity. When the electron density generated by photoionization reaches a high density (e.g., $\omega_p \sim \omega \sim 10^{21}\,\mathrm{cm}^{-3}$), a large fraction of the remaining femtosecond laser pulse can be absorbed.

It is interesting to note that high energy (e.g., three times the bandgap energy) carriers can also be created in materials where the electron–phonon scattering rate is low, such that multiple electron–phonon collisions could not occur in one laser pulse. Carrier heating could be produced through direct interbranch single or multiphoton absorption in a way quite similar to the valence-to-conduction interband absorption discussed above. In all materials, both processes should certainly be taken into account, which one dominates depending essentially on the strength of the electron–phonon coupling.

1.1.3 Avalanche ionization. Avalanche ionization involves free carrier absorption followed by impact ionization (Fig. 1c). As the energy of an electron in the high energy states exceeds the conduction band minimum by more than the bandgap energy, it can ionize another electron from the valence band, resulting in two excited electrons at the conduction band minimum [17, 18]. These electrons can again be heated by the laser electro-magnetic field through free carrier absorption and, once they have enough energy, impact more valence band electrons. This process can repeat itself as long as the laser electromagnetic field is present and intense enough, leading to the so-called electronic avalanche. The growth of the conduction band population by this avalanche process has the form βN, where β is the avalanche ionization rate, a phenomenological parameter that accounts for the fact that only high energy carriers can produce impact ionization.

Avalanche ionization requires seed electrons to be present in the conduction band, which can for instance be excited by photoionization. The following rate equation has been proposed to describe the injection of electrons in the conduction band of dielectrics by femtosecond to picosecond laser pulses, under the combined action of multiphoton excitation and avalanche ionization [19]:

$$\frac{dN}{dt} = aIN + \sigma N I^m ,$$

where a is a constant. For dielectric materials in which free carrier losses (e.g., self-trapping and recombination) occur on a time scale comparable to femtosecond laser pulse duration (e.g., quartz and fused silica), it is likely that this population equation should be modified as follows:

$$\frac{dN}{dt} = aIN + \sigma N I^m + \sigma_x N_{STE} I^{m_x} - \frac{N}{\tau_x} ,$$
$$\frac{dN_{STE}}{dt} = -\sigma_x N_{STE} p I^{m_x} + \frac{N}{\tau_x} .$$

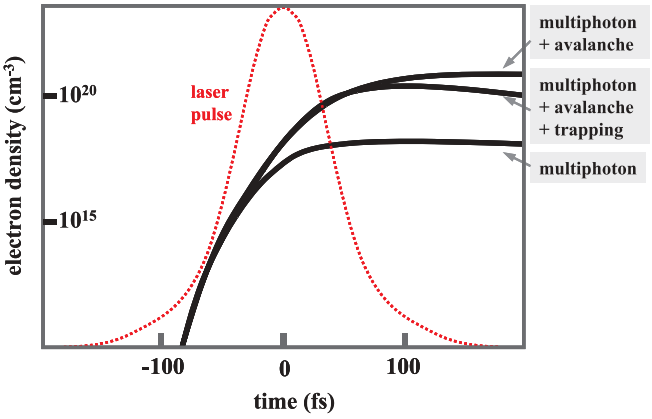

FIGURE 2 Schematic illustration of 100 fs laser-induced electron density evolution under three different excitation-relaxation conditions: multiphoton ionization only, multiphoton plus avalanche ionization, multiphoton plus avalanche ionization with carrier trapping. Multiphoton ionization provides seed electrons for avalanche ionization, whereas trapping offers a channel for electron density reduction. The Gaussian laser pulse is also illustrated

In the above expressions, contribution from self-trapped excitons (Sect. 1.3) of density N_{STE} that builds up during the pulse duration is included (which may in some cases be bimolecular recombination, depending on the carrier density) [20, 21]. σ_x is the multiphoton cross section (of order m_x) for self-trapped excitons and τ_x is the characteristic trapping time. A schematic illustration of the effect of the self-trapping on femtosecond laser excited electron populations is shown in Fig. 2.

More recently, variations of the classical avalanche process that may play a role for sufficiently short laser pulses (e.g., < 40 fs) have been investigated theoretically [22]. One such mechanism is collision-assisted multiphoton avalanche, in which some valence electrons are excited to the conduction band by conduction electrons with energy smaller than the threshold for impact ionization, by absorbing several laser photons during inelastic electron–electron collisions. Another mechanism is hole-assisted multiphoton absorption, which is similar to the so-called enhanced ionization of molecules in strong laser fields [23]. Through its Coulomb field, a hole exponentially enhances the multiphoton absorption rate of atoms at adjacent lattice sites. As soon as new holes are created, they continue the same trend that could lead to a collision-free electronic avalanche.

1.2 *Nonlinear propagation*

When a laser pulse propagates through a dielectric material, it induces microscopic displacement of the bound charges, forming oscillating electric dipoles that add up to the macroscopic polarization. For isotropic dielectric materials such as fused silica, the resulting index of refraction (real part) can be derived as [24]

$$n = \sqrt{1 + \chi^{(1)} + \frac{3}{4}\chi^{(3)} E^2} ,$$

where $\tilde{\chi}^{(1)}$ and $\tilde{\chi}^{(3)}$ are the linear and nonlinear susceptibility, respectively. In a more convenient form,

$$n = n_0 + n_2 I \,,$$

where $I = \frac{1}{2}\varepsilon_0 c n_0 E^2$ is the laser intensity and $n_0 = \sqrt{1+\chi^{(1)}}$ and $n_2 = 3\chi^{(3)}/4\varepsilon_0 c n_0^2$ are the linear and nonlinear part of the refractive index, respectively. A nonzero nonlinear refractive index n_2 (optical Kerr effect) gives rise to many nonlinear optical effects as an intense femtosecond laser pulse propagates through dielectric materials.

1.2.1 Self-focusing and self-phase modulation. The spatial variation of the laser intensity $I(r)$ can create a spatially varying refractive index in dielectrics. Owing to the typical Gaussian spatial profile of a femtosecond laser pulse, the index of refraction is larger toward the center of the pulse. The spatial variation of n causes a lenslike effect that tends to focus the laser beam inside the dielectrics (Fig. 3a). If the peak power of the femtosecond laser pulse exceeds a critical power for self-focusing [24, 25], $P_{\mathrm{cr}} = 3.77\lambda^2/8\pi n_0 n_2$, the collapse of the pulse to a singularity is predicted. Nevertheless, other mechanisms such as defocusing due to nonlinear ionization will always balance self-focusing and prevent pulse collapse inside dielectric materials.

As the result of spatial self-focusing, the on-axis intensity of femtosecond laser pulses inside dielectrics, especially at its temporal peak, can be significantly larger than its original value. Consequently, the pulse may be sharpened (pulse sharpening) temporally with a steeper rise and decay of the temporal profile [26].

Since the intensity $I(t)$ of femtosecond laser pulses is highly time dependent, the refractive index depends on time. Analogous to self-focusing, the phase of the propagating pulse can be modulated by the time-domain envelope of the pulse itself (self-phase modulation). With a nonzero nonlinear refractive index n_2, the derivative of the phase $\Phi(z, t)$ of the pulse with respect to time becomes [24]

$$\frac{\mathrm{d}\Phi}{\mathrm{d}t} = \omega - \frac{n_2 z}{c}\frac{\mathrm{d}I(t)}{\mathrm{d}t} \,.$$

The time-varying term of the phase produces frequency shifts that broaden the pulse spectrum as illustrated in Fig. 3b. Spectral broadening depends on the nonlinear index of refraction n_2 and the time derivative of the laser pulse intensity, and for a time-symmetric pulse the broadening will also be symmetric in frequency. Nevertheless, experimentally observed spectral broadening is seldom symmetric due to processes such as photoionization, which also gives rise to a time-dependent refractive index.

1.2.2 Plasma defocusing. As various nonlinear ionization mechanisms generate an electron–hole plasma inside wide bandgap dielectric materials, this plasma has a defocusing effect for femtosecond laser pulse propagation. The electron density is the highest in the center of the pulse and decreases outward in the radial direction due to the typical Gaussian spatial intensity profile. The real part of the refractive index is modified by the generation of the electron–hole plasma (for $\omega_{\mathrm{p}}/\omega \ll n_0$) [24],

$$n = n_0 - \frac{N}{2n_0 N_{\mathrm{c}}} \,,$$

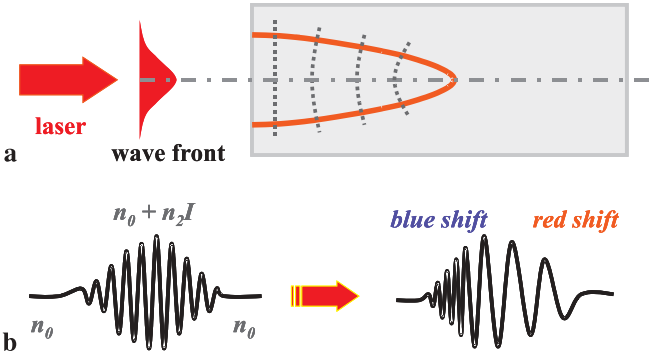

FIGURE 3 Schematic illustration of **a** self-focusing and **b** self-phase modulation resulting from a nonlinear refractive index

where $N_{\mathrm{c}} = \omega^2 \varepsilon_0 m^*/\mathrm{e}^2$, defined as the characteristic plasma density for which the plasma frequency equals to the laser frequency. It is clear that the presence of electron–hole plasmas results in a decrease in the refractive index, in contrast to the optical Kerr effect. As a result, the refractive index is the smallest on the beam axis and the beam is defocused by the plasma, which acts as a diverging lens, possibly balancing self-focusing.

1.3 *Defect generation*

In general, energy from intense femtosecond laser pulses absorbed by a solid material can be converted into elementary electronic excitations – electrons and holes that relax and reduce their energy inside the solid through both delocalized and localized carrier-lattice interaction channels [27, 28]. For some wide bandgap dielectric materials, the most important relaxation mechanism is the localization of the energy stored in the electron–hole pairs that creates self-trapped carriers, especially self-trapped excitons (STEs), which provide energy necessary for localized lattice rearrangement and, thus, defect accumulation.

1.3.1 Excitons. Through nonlinear ionization, the interaction of an intense femtosecond laser pulse with wide bandgap dielectrics causes electronic excitations that promote an electron from the valence band to the conduction band, leaving a hole in the valence band. An electron and a hole may be bound together by Coulomb attraction, which is collectively referred to as an exciton, a concept of electrically neutral electronic excitation [29]. Figure 4 shows a schematic of exciton energy levels in relation to the conduction band edge. While excitons can be either weakly or tightly bound, in wide bandgap materials with a typically small dielectric constant, they are strongly bound and localized near a single atom. Excitons may be promoted by inelastic scattering [30] of the excited electrons that slows the electrons in the conduction band (Fig. 4a) or by direct resonant absorption of multiple photons (Fig. 4b). The binding of electron–hole pairs into excitons is a very fast process that is often shorter than 1 ps in wide bandgap materials [28].

Excitons are unstable with respect to their recombination process; they can relax through delocalized and localized channels. For wide bandgap dielectrics that are strong-coupling solids, a localized trapping mechanism rather than

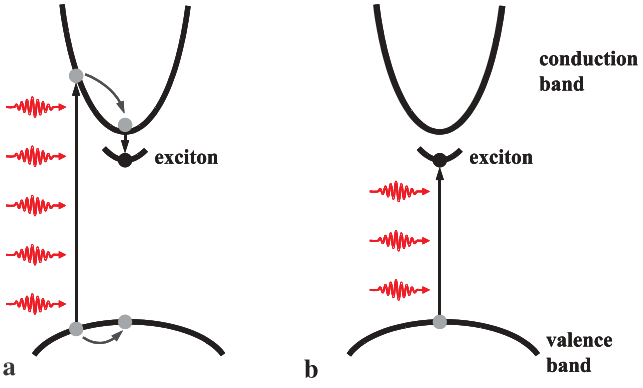

FIGURE 4 Schematic illustration of exciton level and two basic routes for exciton generation. **a** Inelastic scattering of the multiphoton-excited electrons. **b** Direct resonant absorption of multiple photons

scattering is more probable for excitons. Consequently, the electronic excitation energy in these materials is localized by the creation of STE, which is formed as the result of free exciton relaxation or when a self-trapped hole traps an electron [31].

1.3.2 Exciton self-trapping. The major interest in STEs in dielectrics comes from the fact that they are a means of converting electronic excitation into energetic atomic processes such as defect formation. Self-trapping generally describes carriers localized on a lattice site initially free of lattice defects (e.g., vacancies, interstitials, or impurities). It can result from small atomic displacement that deepens the potential well in which the carrier resides. In general, localized lattice deformation may result from short-range covalent molecular bonding or long-range electrostatic polarization associated with ion displacements. Thermal fluctuations can provide the energy for at least one particular lattice site with enough instantaneous deformation for the self-trapping to begin.

Excitons can be trapped by their interactions with lattice distortion to form STEs. Holes may also be trapped at the distortion of lattices, which, after trapping an electron, create a STE. Materials that display self-trapping are predominantly insulators with wide bandgaps, such as alkali halide and SiO_2. In alkali halide crystals [32], which have an energy bandgap ranging from 5.9 eV (NaI) to 13.7 eV (LiF), a self-trapped exciton consists of an electron bound by the Coulomb field of the surrounding alkali ions and a hole that occupies an orbital of a halogen molecular ion (X_2^-). Similarly in SiO_2, which is constructed from SiO_4 tetrahedrals with silicon at the center and an oxygen atom at each of the four corners [33], the self-trapping process is accompanied by a strong distortion of the SiO_2 lattice. Weakening of the Si−O−Si bond yields an oxygen atom leaving its equilibrium position in the tetrahedral, forming silicon and oxygen dangling bonds. The hole of the self-trapped exciton stays on the oxygen dangling bond and the electron is on the silicon dangling bond.

Energy transport of STEs is by means of hopping diffusion rather than by band-like mode. As STEs recombine, they produce a characteristic luminescence that can be studied by time-resolved spectroscopy [34–36]. For example, high purity quartz emits a blue luminescence (~ 2.8 eV) under irradiation, which corresponds to a large Stokes shift relative to the bandgap [37]. For wide bandgap dielectric materials, the localized relaxation channel that leads to the production of STEs is correlated with the formation and accumulation of transient and permanent lattice defects.

1.3.3 Origins of intrinsic defects. Optical excitation can be sufficient to generate vacancies and interstitials in perfect dielectric lattices. Defect formation may be classified as extrinsic or intrinsic depending on whether the defect is derived from a precursor. Recent advances [27] in the study of STE structures have provided the basis for a new level of understanding of the mechanisms of intrinsic defect formation. In the absence of exciton self-trapping, electronic excitation would remain completely delocalized in a perfect dielectric material. Exciton self-trapping can provide the energy required (typically a few eV) to initiate intrinsic defects, including vacancy-interstitial pairs where an atom is displaced in the course of the decay of electronic excitations.

Excitonic mechanisms of defect formation are well established in laser-irradiated halides and SiO_2, among many other wide bandgap materials with strong electron-lattice couplings. F-centers and H-centers [27] are the primary defects that are the immediate products of self-trapped exciton decay in alkali halides (Fig. 5). After initial nonlinear ionization that generates electrons and holes, the process of defect formation starts from exciton creation, followed by self-trapping of the exciton. An isomeric transformation occurs from a self-trapped exciton to a Frenkel defect pair comprising an F-center, a halogen vacancy with a bound electron, and an H-center, an interstitial halogen ion bound to a lattice halogen ion by a hole. Off-center relaxation is the crucial step toward decomposition of the self-trapped exciton, as a self-trapped exciton is gradually changed to a stable vacancy-interstitial defect pair by displacing the H-center away from its point of creation, out of the range for recombination with the electron wave function bound to the F-center.

In SiO_2, the E′ (oxygen vacancy) and nonbridging oxygen-hole centers (NBOHC) [27] are the analog of the F-H centers in alkali halides (Fig. 6). The oxygen vacancy in SiO_2 is essentially a dangling silicon bond [$Si^{\bullet}$]. The displaced oxygen atom goes into the nonbridging oxygen-hole center state [Si-$O^{\bullet}$], which may end up in a peroxy linkage [Si-O-O-Si] or radical [Si-O-$O^{\bullet}$], an isomer of a self-trapped exciton after covalently coupling to another oxygen atom at an interstitial

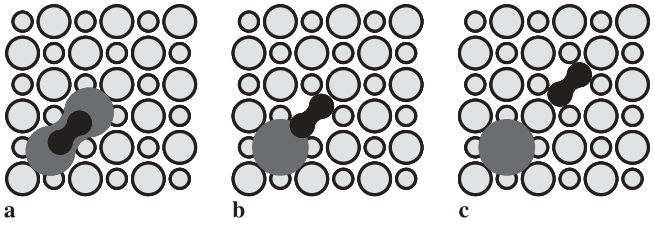

FIGURE 5 Schematic illustration of defect formation from self-trapped excitons. **a** On-center self-trapped exciton. **b** Off-center self-trapped exciton. **c** F−H pair in alkali halides. *Small* and *large circles* represent alkali and halogen ions, respectively

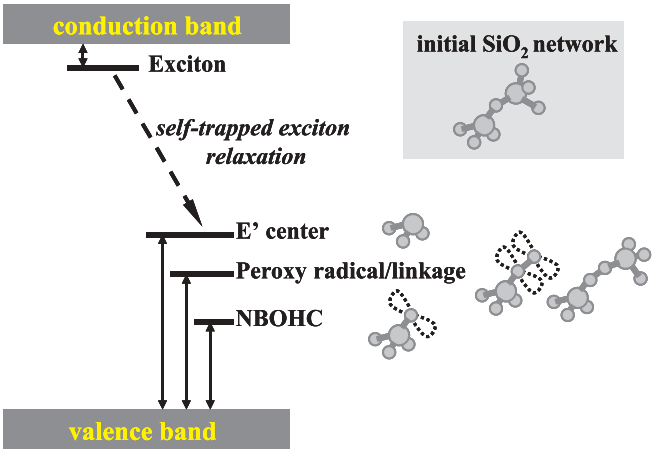

FIGURE 6 Schematic illustration of exciton and intrinsic defect energy levels in SiO_2

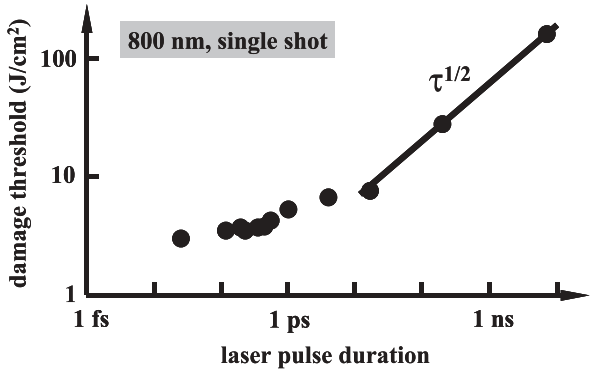

FIGURE 7 Femtosecond (800 nm) laser-induced damage threshold in fused silica. Data from reference [39]

site. Figure 6 also shows a simplified energy level diagram of SiO_2 (silica) upon laser irradiation. The point defects resulting from decay of self-trapped excitons add more energy levels, in analog to the effect of impurities.

As a result of intense femtosecond laser irradiation, when the electronic defects resulting from the decay of self-trapped excitons grow in number, defect clusters may form, which can yield macroscopic structural damage in the material. In addition, significant transient volume increase associated with exciton self-trapping could create a shockwavelike perturbation that eventually damages the otherwise perfect lattice.

1.3.4 Damage of dielectrics. Laser-induced damage in wide bandgap dielectric materials is known to be an extremely nonlinear process. There is no doubt that damage in pure wide bandgap materials is associated with rapid buildup of conduction electrons. A large number of experimental and theoretical studies have been performed to determine the damage mechanisms, with a majority of these efforts focused on the damage or breakdown threshold as a function of the laser pulse duration. It is well established that for pulse durations of 10 ps or longer when thermal diffusion comes to play, the threshold laser fluence (energy density) for material damage depends on laser pulse duration [19, 38, 39] following a $\sqrt{\tau_{\text{laser}}}$ scaling. Nevertheless, for femtosecond laser interactions with wide bandgap dielectrics, when the pulse duration is much shorter than the characteristic time for thermal diffusion, the damage threshold deviates from such square root scaling (Fig. 7).

There have been many theoretical and experimental attempts [19, 39, 40] aimed at determining the mechanism of femtosecond laser-induced dielectric breakdown. The primary goal of these studies has been to determine the relative role of the different ionization and relaxation channels in femtosecond laser-induced dielectrics breakdown, particularly near the damage threshold. Despite these extensive studies, the issue, especially the relative role of multiphoton and avalanche ionization in the generation of the electronic excitation, is far from fully understood.

Once an electronic excitation is generated, several mechanisms can be foreseen that may lead to damage or optical breakdown of a defect-free dielectric material under femtosecond laser excitation. Damage could be caused by melting or vaporization of the solid, following strong phonon emission induced by the laser-generated conduction electrons. Coulomb explosion was also proposed as a mechanism to explain single-shot ablation by femtosecond laser pulses [41, 42]. This hypothesis is supported by the measurement of the velocity of doubly charged ions O^{2+}, which is twice the velocity of singly charged ions (O^+) in the damage of Al_2O_3 [41]. It is well known that single-shot and multiple-shot ablation thresholds differ by a factor of approximately two. This suggests that the first laser shots induce a large concentration of defects in the material lattice that modifies the interactions of the subsequent pulses. In this case, the energy distribution of ions at the surface does not correspond to Coulomb explosion [41] but rather to a Maxwell–Boltzmann distribution, indicating a thermalization process within the dense plasma before desorption.

Damage can also be due to the outcome of generation and accumulation of intrinsic defects such as vacancy-interstitial pairs. As discussed earlier, creation and decay of STEs in dielectrics are at the origin of the intrinsic defects. Theoretical models that describe femtosecond laser-induced optical breakdown in perfect dielectrics should implement the evolution of excitons (formation, self-trapping, and relaxation), as well as different ionization and delocalized recombination mechanisms. No such comprehensive model exists to the best of our knowledge [43].

In the next two sections, we will provide more detailed accounts of some recent progress on two related subjects, femtosecond laser-induced carrier dynamics and femtosecond laser pulse propagation in dielectrics.

2 Femtosecond laser-induced carrier dynamics

2.1 *Imaging experiments*

One simple method to study femtosecond laser-induced carrier excitation in (transparent) dielectrics is ultrafast imaging. Experiments [44] were performed using a femtosecond time-resolved pump-probe setup to image the electron–hole plasma. A high-power femtosecond laser at its fundamental wavelength (800 nm) was used as the pump beam, which has a duration of approximately 100 fs (FWHM). The 800 nm laser beam was focused to a spot size of 50 μm in diameter onto a silica glass sample using an $f = 15$ cm focal-length lens. After a beam splitter, one

arm of the 800 nm output passes an optical delay stage and a KDP crystal, forming a probe beam at 400 nm that is perpendicular to the excitation laser pulse. By moving the delay stage, the optical path of the probe beam can be varied, so the time difference between the pump beam and the probe beam is changed. Time zero was set when the peaks of the ablation laser beam and the probe beam overlapped in time at the sample surface. The resulting shadowgraph images represent spatial transmittance of the probe pulse during laser irradiation of the sample, corrected for background intensity measured without laser excitation. Electron number density of the laser-induced plasma inside the silica can be estimated from the transmittance at various delay times.

Figure 8a shows a series of time-resolved images of the electron–hole plasma at the same laser irradiation $I = 1.3 \times 10^{13}\,\mathrm{W/cm^2}$. At $t = 0$, only a small dark area appears close to the glass surface that results from electron excitation by the leading edge of the femtosecond laser pulse. At longer delay times, plasma filament grows longer, with the darkest section (strongest absorption) moving away from the glass surface into the bulk. From measuring the probe pulse transmittance of the time-resolved images, one can estimate the femtosecond laser-excited plasma electron number density inside the silica glass at different delay times.

The electron number density of the laser-induced plasma shown in Fig. 8a was plotted in Fig. 8b. At $t = 333$ fs, there is an electron number density maximum ($\sim 2 \times 10^{19}\,\mathrm{cm^{-3}}$) at $z = 80\,\mu$m that moves into the silica at later times. While the peak value of the electron number density increases with time, it reaches a maximum of approximately $5 \times 10^{19}\,\mathrm{cm^{-3}}$ at $t = 1333$ fs. This observation is consistent with the fact that a femtosecond laser pulse experiences initial self-focusing inside a dielectric material, followed by defocusing when the laser-induced electron excitation is strong enough to compensate the laser-induced refractive index change.

The density of the laser-induced electron–hole plasma as obtained from ultrafast imaging provides only an order-of-magnitude estimate or semiquantitative information of laser-interactions with dielectrics. Frequency domain interferometry proves to be a powerful technique for elucidating the fundamental processes of femtosecond laser-induced carrier dynamics in dielectric materials.

2.2 *Interferometry experiments*

While imaging experiments give access to the change of the imaginary part of the refractive index induced by a pump laser pulse, the change in the real part of the refractive index also provides essential information on the dynamics of excited carriers in dielectrics. Interferometry is the natural tool to access this quantity. A very powerful interferometric technique when dealing with broadband light sources is spectral interferometry, which has been increasingly implemented with ultrashort laser pulses for a wide variety of experiments, e.g., for the full temporal characterization of these pulses (SPIDER technique) [45, 46] or for time-resolved experiments, especially in laser-generated plasmas [47]. Note that a technique combining the features of interferometric measurements (in real space) and that of shadowgraphy [48] has also been implemented in the case of picosecond pulses and could, in principle with minor modifications, be applied to femtosecond pulses.

The spectral or frequency domain interferometry technique uses two pulses, separated in time by a delay τ that is large compared to their duration and sent to a spectrometer. Provided the spectral resolution of the spectrometer is much

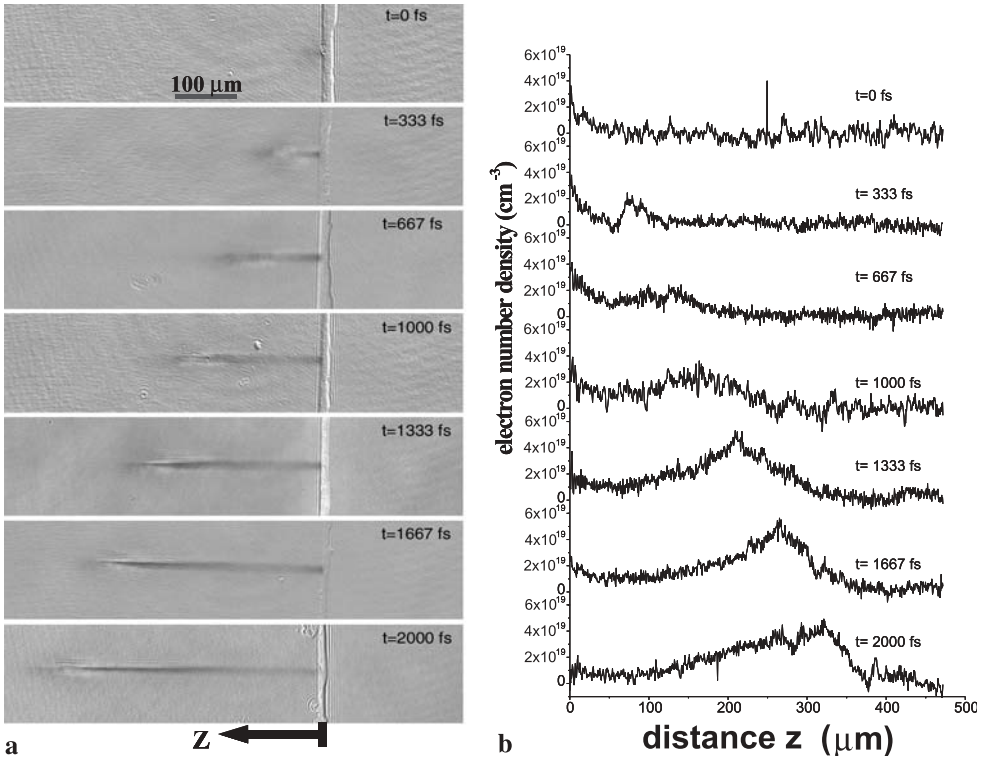

FIGURE 8 **a** Time-resolved images of femtosecond laser-induced electronic excitation inside a silica glass. **b** Evolution of electron number density profile inside a femtosecond laser-irradiated silica glass

larger than the inverse of the delay, the measured spectrum is therefore

$$S(\omega) = 2S_0(\omega)[1 + \cos(\omega\tau + \Phi)] .$$

For simplicity, the two delayed pulses were assumed to be identical ("twin pulses") to derive this expression, a condition that is actually not required for this technique to apply. $S_0(\omega)$ is the spectral intensity of these pulses and Φ their relative phase. Since τ is large compared to the spectral width of $S_0(\omega)$, $S(\omega)$ presents fringes, spaced by $2\pi/\tau$. The position of these fringes is determined by the relative phase Φ of the two pulses.

Spectral interferometry can be used to probe the temporal dynamics of a system perturbed by a pump pulse. In this case, the first pulse probes the system before the pump pulse and is thus used as a reference pulse. The second pulse probes the system at a delay t after the pump pulse. The perturbation induced by the pump pulse leads to a change $\Delta\Phi(t)$ of the relative phase of the twin pulses. This phase shift $\Delta\Phi$ results in a shift of the fringes in the spectrum of the twin pulse. Spectral interferometry uses this shift to measure $\Delta\Phi$. This technique has been used to probe laser-excited dielectrics (Fig. 9) [49]. The twin pulses are transmitted through the dielectric sample. One interferogram is acquired without any pump pulse, as the reference. A second one is measured with an intense pump pulse exciting the dielectric between the reference and the probe pulse. In this configuration, the phase shift $\Delta\Phi(t)$ is given by

$$\Delta\Phi(t) = (2\pi L/\lambda)\Delta n(t),$$

where λ is the probe beam wavelength, L the length of the probed medium (assumed to be homogeneously excited for simplicity), and $\Delta n(t)$ the instantaneous change in the real part of refractive index that results from the pump-induced excitation. Note that, by using the contrast of the fringes, spectral interferometry also gives access to the change in absorption coefficient, i.e., to the change in the imaginary part of the refractive index.

Two types of temporal behavior of $\Delta\Phi(t)$ have been observed (Fig. 10). In all cases, $\Delta\Phi(t)$ is positive for short delays, when the pump and the probe temporally overlap in the dielectric, because of the pump-induced optical Kerr effect. $\Delta\Phi(t)$ then becomes rapidly negative; according to the Drude model, it is due to the injection of electrons in the conduction band (Sect. 1, plasma defocusing). In some solids (e.g., MgO in Fig. 10), $\Delta\Phi(t)$ remains negative for several tens of picoseconds, while in others (e.g., SiO_2 in Fig. 10) it becomes positive again. In SiO_2, this relaxation occurs with a time constant of 150 fs. It has been demonstrated that this second type of evolution is due to the trapping of most of the excited carriers as self-trapped excitons [49]. Since STEs correspond to localized states, the change in the refractive index is given by the Lorentz model

$$\Delta n = \frac{N_{\mathrm{STE}}\, e^2}{2n_0 m\varepsilon_0}\,\frac{1}{\omega_{\mathrm{tr}}^2 - \omega^2},$$

where N_{STE} is the STE density, n_0 the refractive index of the unperturbed solid, ω_{tr} the resonance frequency of the STE's

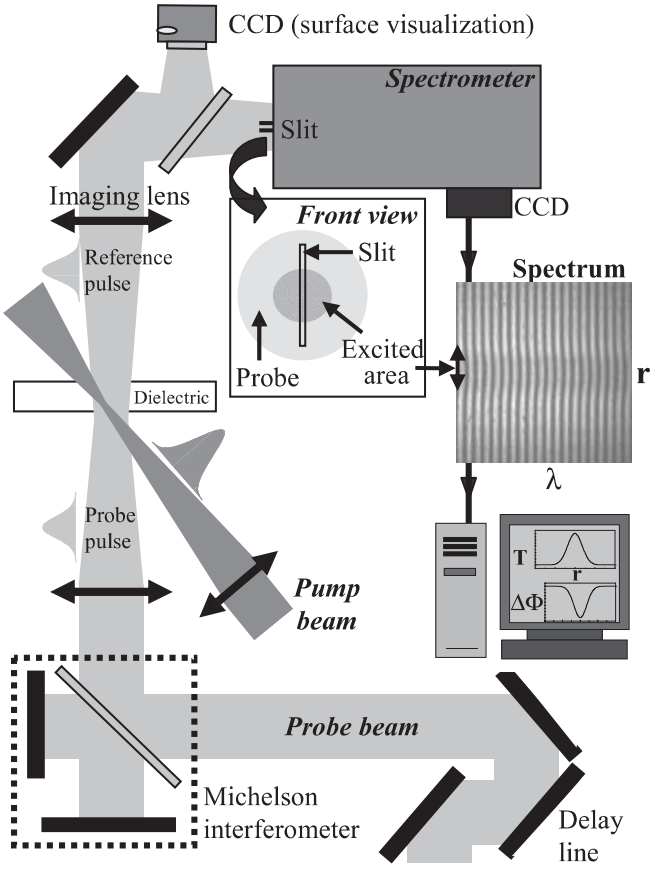

FIGURE 9 Experimental setup for spectral interferometry. The probe beam waist is larger than the pump beam waist (typically 10 μm), and the interaction area is imaged on the entrance slit of the spectrometer with a large magnification, so that the spatial profile of phase shift along the slit direction (r) is obtained

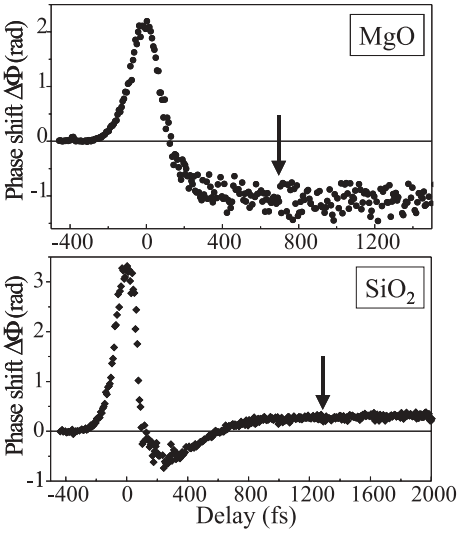

FIGURE 10 Temporal evolution of phase shift in MgO and SiO_2 (800 nm pump with an intensity well below the breakdown threshold, 400 nm probe). The *arrows* indicate the delays where the intensity dependences of phase shift in these two materials were measured

first excited level (~ 4.2 eV in SiO_2), and ω the probe laser central wavelength. If $\omega < \omega_{\mathrm{tr}}$, as is the case for the SiO_2 data in Fig. 10, the presence of STEs leads to a positive phase shift.

These measurements have provided important information on the ultrafast dynamics of excited carriers in dielectrics [49]. In diamond, MgO and Al_2O_3, the negative phase shift was observed to persist for tens of picoseconds. This suggests that no trapping occurs on this timescale or that the electrons form very shallow traps. Fast formation of STEs has been observed in NaCl, KBr, and SiO_2 (both amorphous and crystalline), leading to carrier lifetimes two orders of magnitude smaller. The difference in carrier dynamics can be qualitatively explained by general considerations about STE formation in terms of lattice elasticity and deformation potential. A fundamental difference was also observed between the trapping kinetics in NaCl and SiO_2: while the trapping time was independent of the excitation density in SiO_2, carriers in NaCl trap faster when the excitation density is higher. This can be interpreted as evidence of direct exciton trapping in SiO_2 and of hole trapping followed by electron trapping in NaCl [49].

For intense ultrashort laser interactions with dielectrics [50], the phase shift $\Delta\Phi_\infty$ measured at a sufficiently large delay after the laser pulse (see arrows in Fig. 10) gives access to the excitation density N in the solid at the end of the laser pulse. If this density is not too high, $\Delta\Phi_\infty$ is directly proportional to N. Figure 11 presents the evolution of $\Delta\Phi_\infty$ with the incident peak intensity I of a 790 nm ($\omega = 1.57$ eV), 60 fs pump pulse, in two dielectric solids. On the right-hand scale, the corresponding excitation density N is given, assuming a homogeneously excited medium. At low intensity, $\Delta\Phi_\infty$ is observed to vary as I^6 in SiO_2 and as I^5 in MgO. The exponents of these power laws correspond in both cases to the minimum number of photons that the valence electrons have to absorb to be injected in the conduction band ($6\omega = 9.42\,\text{eV} > E_g(SiO_2) \approx 9\,\text{eV}$, $5\omega = 7.85\,\text{eV} > E_g(\text{MgO}) \approx 7.7\,\text{eV}$). This proves that the dominant excitation process in this intensity range is perturbative multiphoton absorption by valence electrons. The optical breakdown threshold of SiO_2 measured at 800 nm and 60 fs in [19] falls within this range, suggesting that optical breakdown is not associated with an electronic avalanche. However, this result is in contradiction with the conclusions drawn from breakdown threshold measurements [19], which suggest that the electronic avalanche should dominate multiphoton absorption even in the femtosecond regime. A model of optical breakdown conciliating these two studies remains to be found.

At higher intensities, a saturation of $\Delta\Phi_\infty$ is observed compared to these power laws. This saturation occurs because at high intensity, the pump beam is strongly absorbed due to free-carrier absorption by conduction electrons and even reflected by the target when the electron density becomes higher than the critical density at the pump frequency. Thus, in this regime, it is only in a thin layer (~ 200 nm) of material that the excitation density keeps increasing with intensity. In this range, the occurrence of electronic avalanche, due to the strong heating of the conduction electrons, cannot be excluded, although the data can be fitted with a purely multiphoton injection law [50]. Since the density only increases with intensity in a very thin layer, the sensitivity of the technique to these variations might be too low to distinguish between different excitation processes.

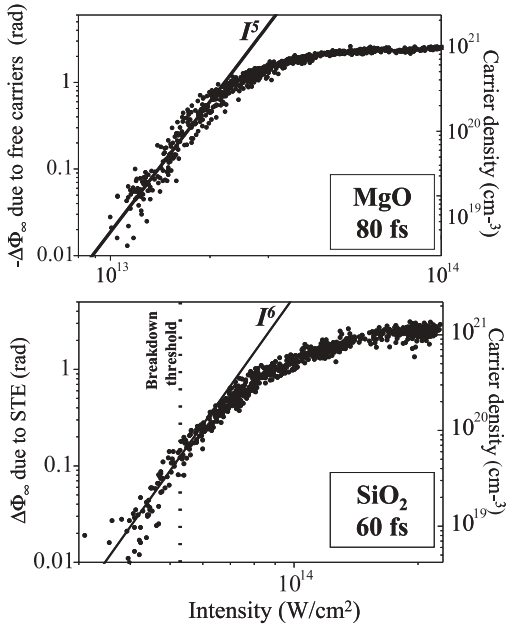

FIGURE 11 Intensity dependence of the phase shift ($\Delta\Phi_\infty$) after the pump (see *arrows* in previous figure), for an 800 nm pump, in MgO and SiO_2. The *full lines* indicate the power laws obtained at low intensity. The *vertical dotted line* shows the breakdown threshold measured in SiO_2 for a 60 fs, 800 nm pulse [19]

2.3 *Time-resolved absorption*

STE creation by self-trapping of an electron–hole pair can be monitored using transient absorption spectroscopy, which consists of measuring the sample absorption at different delay after electron–hole injection and monitoring the appearance of selected absorption bands. In some dielectric materials such as SiO_2, for which the absorption lies in the UV, it is only possible to perform single wavelength measurements [36]. Figure 12 shows the rise time of the SiO_2 STE absorption measured at the top of its 5.2 eV absorption band.

In alkali halides, where the absorption bands lie in the visible, it is possible to use as a probing pulse a white light continuum (WLC) generated by focusing an intense subpicosecond laser pulse in, e.g., a water cell. Due to various nonlinear effects (Sect. 3.3), the spectrum of the laser pulse is broadened and can essentially cover the whole visible range so that a full absorption spectrum can be recorded simultaneously for each laser shot.

Figure 13 shows such absorption spectra measured in KCl, at two temperatures [51]. At 6 K, one observes the appearance of a single absorption band that can be shown to relate to the STE formation (just as in the case of SiO_2 above). At 80 K, at short delays, one also observes the appearance of the STE absorption, but after a few picoseconds a second band appears. This is due to the transformation of some of the STE into a permanent F-center. This method has now been applied to a large number of alkali halides [52, 53] and has considerably helped, together with the above-mentioned interferometric measurements, unravel the difficult issue of the so-called "excitonic" mechanisms of point defect creation in laser-irradiated wide bandgap dielectrics.

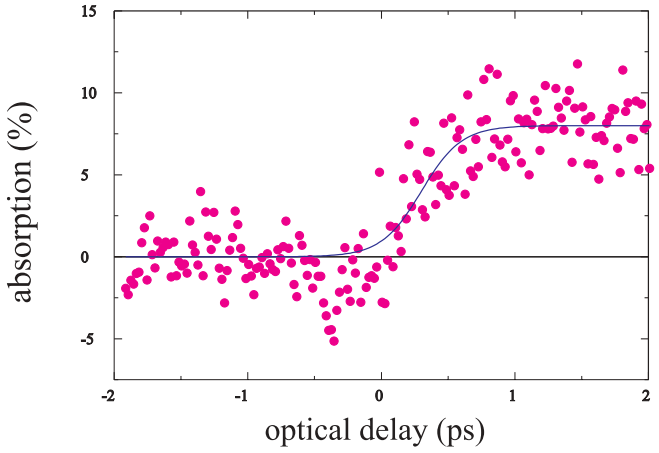

FIGURE 12 Rise time of the 5.2 eV absorption band of the SiO_2 STE

2.4 *Theoretical considerations*

While experimental detection of laser-induced ultrafast carrier dynamics advances rapidly, theoretical calculation of the dynamics in strong-coupling solids is still limited. One primary challenge is the appropriate approach to calculating nonequilibrium carrier distributions in dielectrics in response to intense femtosecond laser excitation.

The main difficulty comes from the very strong electron–phonon coupling in the conduction band of wide bandgap dielectrics, which is an important feature of these materials. For the longitudinal optical (LO) phonons, this coupling is measured with the well-known quantity α defined as

$$\alpha = \frac{e^2}{\hbar}\left(\frac{m^*}{2\hbar\omega_{LO}}\right)^{1/2}\left(\frac{1}{\varepsilon_\infty}-\frac{1}{\varepsilon_0}\right).$$

It depends [54] on the dielectric properties of the material (ε_0, ε_∞), the LO phonon energy at the center of the Brillouin zone (ω_{LO}), and the electron effective mass (m^*). Its value ranges from 6×10^{-2} for semiconductors such as GaAs (perturbative regime) to larger than unity for SiO_2, and even 5 for NaCl.

To calculate the temporal evolution of a given electron distribution function corresponding to an energy in excess with respect to the bottom of the conduction band, one generally uses the so-called Boltzmann equation approach. This semiclassical approach implies the acceptance of two very strong hypotheses. First, one must first suppose that the evolution process is Markovian, i.e., the evolution of the system after t depends only on its state at this time and not before (the system has no memory). Second, it is necessary to calculate a mean time-independent collision rate $W(\boldsymbol{k},\boldsymbol{k}')$ with the Fermi golden rule, which gives the probability per unit of time for the system to reach a state $\boldsymbol{k}'$ starting from $\boldsymbol{k}$ and implies a strict energy conservation.

For the case of quartz [55], to simplify the discussion, we neglect any exchange and correlation interactions among electrons, as well as the Coulomb interaction with the holes, the trapping process, interactions with impurities, and, owing to relatively low electronic density, all degeneracy effects. The evolution equation is written

$$\frac{\delta f(\boldsymbol{k},t)}{\delta t} = \int \mathrm{d}\boldsymbol{k}\,\left\{W(\boldsymbol{k}',\boldsymbol{k})\,f(\boldsymbol{k}',t) - W(\boldsymbol{k},\boldsymbol{k}')\,f(\boldsymbol{k},t)\right\}.$$

This equation, also called the master equation, makes for each time the balance between the population and depopulation of the states $\boldsymbol{k}$ of the system [56].

We consider as an example a seven-photon injection process (1.57 eV photons) in a quartz sample with bandgap of 9.8 eV. Then, the initial kinetic energy of the electrons in the conduction is about 1.2 eV. We want to focus on the relaxation of these electrons through electron–phonon coupling, and we therefore neglect the influence of the laser electromagnetic field (and in particular free-carrier absorption), assuming that this field is quickly switched off. We consider only the two most active LO phonon branches (150 meV and 60 meV), assuming a flat dispersion curve. The coupling is calculated using the well-known Fröhlich [57] Hamiltonian, and the transition rates are obtained, as discussed above, using the Fermi golden rule. The energy is lost by quanta corresponding to the two considered branches. The equilibrium is reached after 50 fs (Fig. 14), and it corresponds to a Maxwell–Boltzmann distribution (defined as an exponential with a mean energy $3/2k_BT$).

At this stage, an important comment is necessary: the semiclassical approach has, by construction, no memory. A description based on this assumption is correct if an event (a collision with a phonon) is over before the next one starts. The collisions must then be successive and independent. This

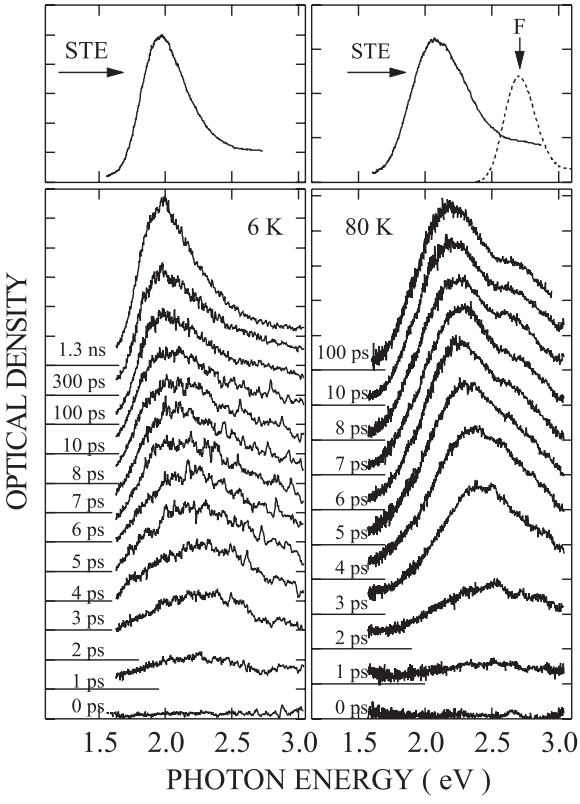

FIGURE 13 Typical time-resolved absorption spectra measured in KCl at two temperatures. At 6 K, only the STE absorption is observed, while at 80 K one sees evidence of the transformation of some STE in a permanent F-center [51]

is not true in the case of conduction electrons in SiO_2; because of the strong electron–phonon coupling (large α), the mean collision time τ is smaller than 1 fs. We can also calculate the "duration" of a collision as the time required for the energy to be conserved. For the 150 meV branch, we find $1/\omega_{\mathrm{LO}} \sim 5$ fs. According to these two parameters, a collision starts before the end of the previous one. This strongly suggests that the semiclassical approach no longer applies.

The full quantum approach based on the evolution of the density matrix does not require energy conservation at each collision. In addition, a Markovian assumption is no longer necessary. This approach has been utilized in the case of semiconductors and is detailed in [58]. One generally starts from the single particle density matrix evolution equation:

$$\frac{\mathrm{d}}{\mathrm{d}t}\left\langle c_k^+ c_k\right\rangle = \frac{1}{i\hbar}\left\langle\left[c_k^+ c_k, H\right]\right\rangle .$$

H is the Fröhlich Hamiltonian and $\left\langle c_k^+ c_k\right\rangle = f(k)$ is the distribution function that we want to calculate. It is well known that the set of equations derived from the above evolution equation is infinite [59]. Strictly speaking, the problem cannot be computed. We must truncate the set of coupled differential equations somewhere. In the calculation detailed in [55], the average of a product of four operators (two for the electrons and two for the phonons) has been factorized in two products of two operators, each acting, respectively, on the electron and the phonons: $\left\langle c_{k+q-q'}^+ c_k b_q^+ b_{q'}\right\rangle = f(k) n_q \delta_{qq'}$. In this expression, b_q^+ ($b_{q'}$) is the operator for the creation (destruction) of a phonon $q(q')$. Because we consider that the average of a product is the product of the average, this is equivalent to neglecting the fluctuations in establishing equilibrium. The difference between this approach and the semiclassical one is illustrated in Fig. 14. It clearly takes more time in the quantum approach for the carriers to relax. This is understandable because, as the memory is conserved, it takes more time to reach an equilibrium state that is by definition universal and thus free of memory.

The above example underlines the tremendous challenge that one faces in properly calculating the evolution of an electronic distribution in a nonequilibrium state under the condition of strong coupling. Even in this oversimplified model, where a simple parabolic dispersion relation for the electrons and a flat one for the LO phonons are applied, it is not an easy task, from the practical as well as conceptual point of view, to calculate ultrafast carrier dynamics. There is a need for developing a microscopic theory based on the quantum approach that quantitatively describes the ultrafast carrier dynamics resulting from femtosecond laser excitation in dielectrics.

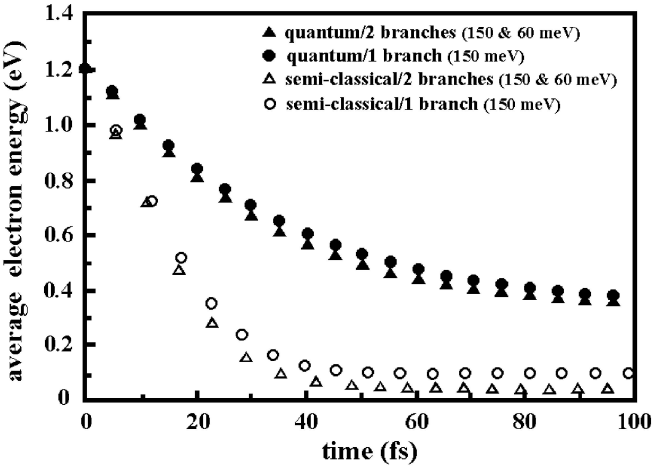

FIGURE 14 Comparison of semiclassical and quantum approaches in calculating average electron energy as a function of time

Recent progress of ab initio electronic structure calculations [60] offers some hope concerning electronic excitation in dielectrics. This approach can quite accurately reproduce experimental properties such as photoabsorption, photoemission, or electron energy loss spectra, all properties pertaining to the excited states, without the use of any adjustable parameter. Many-body quantum calculations presently can determine the real part of quasiparticle (in our case, laser-excited carrier) self energy; it is only a matter of time before the corresponding imaginary part, which will provide a solution to the problem that accounts for all electron–electron and electron–hole relaxation processes, is obtained. Electron lattice interactions are not currently included in such formalisms, but they could be accounted for once some recent methodological progress in the field of time-dependent density functional theory (TDDFT), a general framework for studying nonstationary electronic processes [61], are to be fully exploited.

3 Femtosecond laser pulse propagation

There has been a growing interest in femtosecond laser propagation in wide bandgap dielectrics as the laser power can be much higher than the threshold for self-focusing. At such high intensities, the dynamics of femtosecond pulse propagation is considerably more complex, as it may be accompanied by nonlinear phenomena such as pulse splitting in both space and time domains. Spatial or temporal splitting of femtosecond laser pulses offers a mechanism for intense femtosecond laser propagation inside dielectrics without encountering catastrophic damage caused by self-focusing (Sect. 1.2).

3.1 *Self-focusing and defocusing*

Femtosecond laser-induced nonlinear self-focusing as well as the related filamentation process has been investigated for decades, for example, in air [62, 63]. The nonlinear Schrödinger equation with the inclusion of multiphoton ionization can describe many aspects of the filamentation phenomenon [64]. However, there are relatively few femtosecond time-resolved studies of laser self-focusing and filamentation inside wide bandgap dielectrics. Figure 8 provides direct evidence for strong self-focusing of a femtosecond laser pulse inside a silica glass at different times. The width of the filaments decreases as the laser pulse propagates into the sample.

Although self-focusing occurs during femtosecond laser propagation, the density of free electrons at the focus does not increase indefinitely. Rather, the density reaches a saturation value after about 1500 fs propagation into the sample

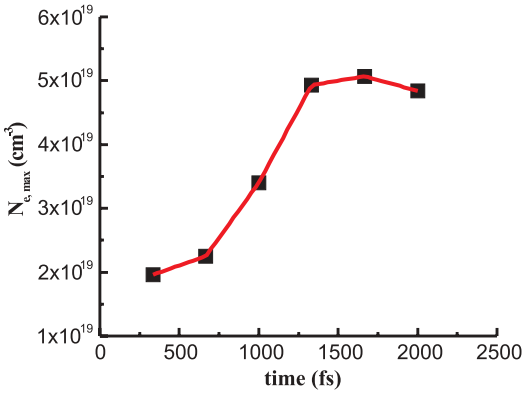

FIGURE 15 Maximum electron density as a function of time as a femtosecond laser pulse (100 fs, 800 nm) propagates inside a silica glass

(∼ 250 μm inside), as shown in Fig. 15. This phenomenon happens to be the consequence of self-defocusing process caused by the generation of an electron–hole plasma, as discussed in Sect. 1.2. The balance between self-focusing due to the nonlinear optical Kerr effect and defocusing due to plasma formation can lead to self-channeling of the femtosecond laser pulse inside dielectrics [65, 66] if the beam radius is such that ionization comes into play before spatial splitting and material damage occur.

3.2 *Spatial splitting*

When self-focusing is strong, a single input femtosecond laser pulse can break up into several narrow filaments of light. Because the Gaussian spatial profile of the pulse is destroyed by self-focusing, the pulse cannot be focused to a diffraction-limited size. Figure 16 shows a series of shadowgraph images inside a silica sample taken at the same delay time (2000 fs) but at different laser intensities I. At $I = 5 \times 10^{12}\,\mathrm{W/cm^2}$, there is only one filament, a thin, dark stripe that results from the absorption of the probe beam by laser-excited electrons inside the silica glass. At $I = 2.5 \times 10^{13}\,\mathrm{W/cm^2}$, the primary filament splits into two at a location about 200 μm inside the silica glass. At even higher irradiance (e.g., $10^{14}\,\mathrm{W/cm^2}$), filament splitting, as a persistent phenomenon, starts right after the femtosecond laser pulse enters the glass sample.

The nonlinear Schrödinger equation, which is the leading order approximation to the Maxwell equations, has been successful in describing the propagation of intense laser pulses such as self-focusing in nonlinear Kerr media with nonlinear refractive index n_2. Assuming the laser pulse propagates in the z direction, the basic nonlinear Schrödinger equation has the form [24]

$$2ik\frac{\partial A}{\partial z} + \nabla_\perp^2 A + \frac{2k^2 n_2}{n_0}|A|^2 A = 0\,,$$

where A is the envelope amplitude of the propagating laser electric field, k is the wave vector, $k = \omega n/c$, and $\nabla_\perp^2$ is the transverse Laplacian operator. The second term represents diffraction, whereas the third term accounts for the contribution due to the intensity-dependent refractive index. If the input laser pulse is cylindrically symmetric, according to the nonlinear Schrödinger equation, the pulse remains cylindrically symmetric during propagation. As the interpretation of multiple filamentation should include a mechanism that breaks the cylindrical symmetry, the standard explanation of multiple filamentation, developed nearly 40 years ago [67], is that breakup of cylindrical symmetry is initiated by small or random inhomogeneity in the input laser pulse. According to this theory, which was based on modulational instability of plane waves that allowed exponential growth of initial perturbations, there is a preferred spatial scale for filaments to form, depending on laser intensity [67].

An alternative deterministic explanation of filament splitting was proposed recently [68] based on the nonlinear

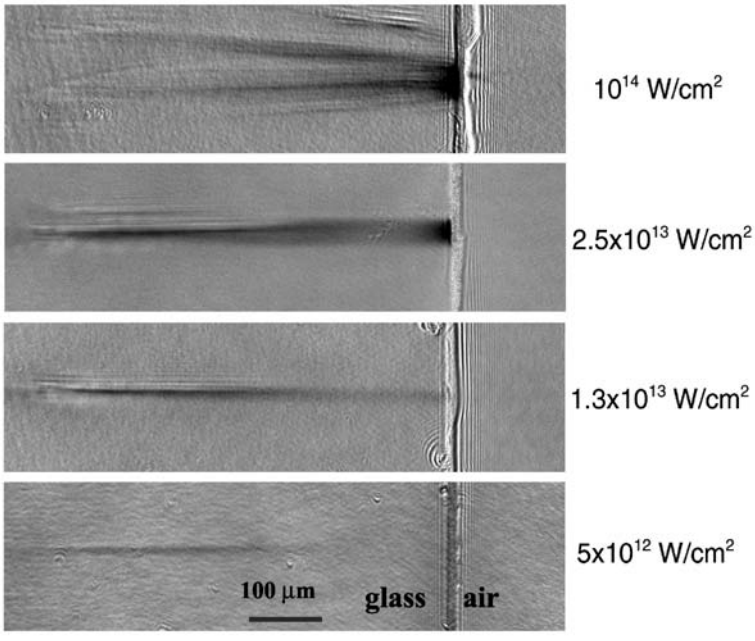

FIGURE 16 Intensity dependence of femtosecond laser-induced electronic excitation inside a silica glass

Schrödinger equation with the inclusion of nonlinear perturbation that describes self-focusing in the presence of vectorial (polarization) as well as nonparaxial effects. Assuming the input laser pulse is linearly polarized in the x direction, the general form of the modified nonlinear Schrödinger equation can be derived as [68]

$$2ik\frac{\partial A}{\partial z}+\nabla_{\perp}^{2}A+\frac{2k^{2}n_{2}}{n_{0}}|A|^{2}A = f^{2}\,\mathrm{Im}\left(A,\frac{\partial A}{\partial x},\frac{\partial^{2}A}{\partial x^{2}}\right)+O\left(f^{4}\right),$$

where $f(\ll 1)$ is the dimensionless parameter defined as the ratio of the laser wavelength to the pulse spot parameter, $f=\lambda/2\pi r_0$. The asymmetry in the x and y derivatives of the vectorial perturbation terms in the new equation suggests that the symmetry-breaking mechanism can arise from the vectorial effect for the linear polarized laser pulse. This vectorial-induced symmetry breaking leads to multiple filamentation even when the linearly polarized input laser pulse is cylindrically symmetric. Figure 17 shows a laser pulse profile as it propagates into a Kerr medium at high laser intensity, as calculated using the above modified nonlinear Schrödinger equation [68]. Two filaments emerge that propagate forward in the z direction while moving away from each other along the x direction. Multiple filamentation resulting from noise in the input beam should vary between experiments and be independent of the direction of initial polarization, while multiple filamentation resulting from vectorial effects should persist with experiments and depend on polarization.

3.3 *Temporal splitting*

In addition to spatial splitting, intense femtosecond laser pulse may undergo temporal splitting as it propagates inside a dielectric material [69]. While temporal splitting was predicted theoretically more than 10 years ago [70], experimental verification of temporal splitting occurred within the last decade [71]. In one such experiment [72], a near-Gaussian 78 fs, 795 nm laser pulse was focused at a 75 μm spot size at the front face of a 3 cm long silica glass sample. The temporal behavior of the pulse was characterized by measuring the intensity cross correlation of the transmitted pulse with the initial input pulse. The spectrum of the transmitted beam was taken concurrently using a fiber-coupled spectrometer with 0.3 nm resolution. Figure 18 shows the cross correlation and the corresponding spectrum of the transmitted pulse on axis for pulse intensity above the threshold power for pulse splitting. Associated with temporal splitting, the spectrum of the femtosecond laser pulse can broaden significantly and eventually evolve into a supercontinuum or white-light generation at high intensities. Although white-light continuum in transparent dielectrics has been known for decades [73, 74], recent systematic experiments have revealed that femtosecond laser-induced continuum generation in dielectrics is triggered by self-focusing and depends strongly on the medium's bandgap [75, 76].

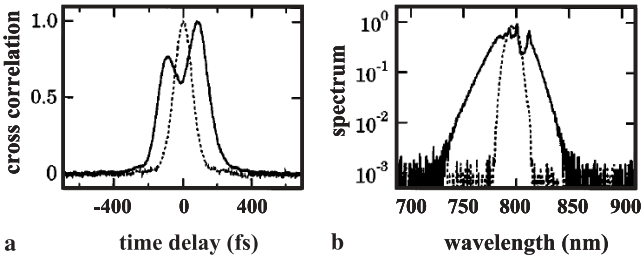

FIGURE 18 Experimentally measured **a** cross correlation and **b** power spectra of a femtosecond laser pulse (78 fs, 795 nm) transmitted through a 3 cm fused silica glass with a peak power 5.1 MW. The *dashed curves* in **a** and **b** are the autocorrelation and the spectrum of the input pulse, respectively [72]

The nonlinear Schrödinger equation with the inclusion of material dispersion was applied to predicting temporal splitting of femtosecond laser pulses inside dielectrics. With the additional group-velocity dispersion term, the nonlinear Schrödinger equation is written [69, 72]

$$2ik\frac{\partial A}{\partial z}+\nabla_{\perp}^{2}A-kk''\frac{\partial^{2}A}{\partial\tau^{2}}+\frac{2k^{2}n_{2}}{n_{0}}|A|^{2}A=0,$$

where k'' is the group-velocity dispersion coefficient, the second derivatives of k with respect to laser pulse frequency, and $\tau=t-z/v_{\mathrm{g}}$ is retarded time for pulse moving at group velocity v_{g}.

Figure 19 shows the calculated pulse intensity surfaces at three propagation distances in fused silica [69]. The femtosecond pulse is initially focused in both space and time as the result of strong self-focusing and the associated pulse sharpening (Sect. 1.2). As the peak intensity increases, the process of self-phase modulation also increases, which leads to the generation of new frequency components that are red-shifted near the leading edge of the pulse and blue-shifted near the trailing edge. Because of positive group-velocity dispersion in most dielectrics, the wave trains of the laser pulse at different frequencies propagate at different speeds, with the red component being faster than the blue. Consequently, the pulse energy is pushed away from $\tau=0$, initiating pulse splitting.

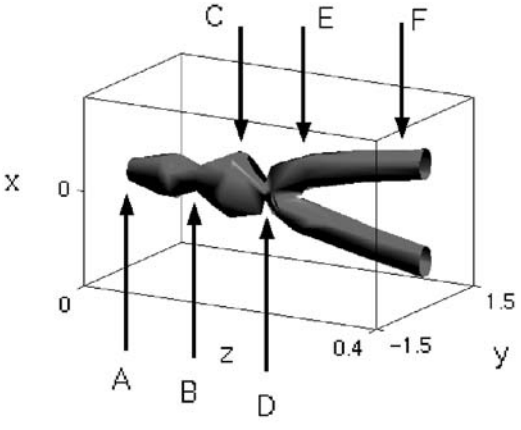

FIGURE 17 Calculated pulse splitting as a femtosecond laser propagates inside a dielectric material. The letters in the figure indicate the propagation distance normalized by diffraction length (A through F: $z=0$, 0.11, 0.14, 0.17, 0.22, 0.4) [68]

While the nonlinear Schrödinger equation including normal group-velocity dispersion predicts temporal splitting with symmetry, the asymmetric feature of the splitting pulses was examined using an equation beyond the slowly varying envelope approximation [72, 77]. Self-steepening and space-time focusing were found to shift the beam energy into one of the two split pulses formed by group-velocity dispersion. Similarly, multiphoton ionization and plasma formation were implemented into the modified nonlinear Schrödinger equation. The resulting defocusing and nonlinear absorption of the trailing edge of the pulse tends to push the peak intensity to the leading edge [78].

4 Concluding remarks

While femtosecond lasers have great potential in processing dielectric materials, the underlying physics is far from fully understood, although significant progress has been achieved in the past few years. We have provided an overview of recent advances in understanding the fundamental processes of femtosecond laser interactions with dielectrics that are important for materials applications. Two topics discussed in this article include the excitation and relaxation channels of femtosecond laser-induced carriers and the splitting and self-focusing/defocusing of femtosecond laser pulses inside dielectrics.

Ultrafast imaging and spectral interferometry techniques have been successfully applied to quantify the dynamics of the laser-excited carriers. A significant advance is the time-resolved detection of exciton self-trapping as a primary de-excitation channel. Such a localized carrier relaxation mechanism offers the possibility of defect formation in some perfect dielectrics. In addition to experiments of ultrafast carrier dynamics, also discussed in this article is the challenge in theoretical calculation of femtosecond laser-excited nonequilibrium carrier distributions in materials involving strong electron–phonon coupling.

Self-focusing, defocusing, and spatial splitting (multifilamentation) of femtosecond laser pulses inside transparent dielectric materials have been examined by ultrafast imaging techniques. In the meantime, splitting of a femtosecond pulse in the time domain has also been reported by different research groups. Recent comprehensive theoretical work based on modifications of the nonlinear Schrödinger equation has provided much insight into the highly nonlinear processes of spatial and temporal splitting of femtosecond laser pulses propagating inside dielectrics.

The selected topics discussed in this article represent two basic research emphases in the growing field of ultrafast laser interactions with dielectrics. With the continuous advancement of ultrashort pulsed lasers, the maturity of ultrafast imaging, interferometry, and spectroscopic techniques, as well as the rapid growth of computing power and the progress in theoretical understanding of the excited states properties of dielectrics, more subtleties of the nonlinear, nonequilibrium processes during and after femtosecond laser excitation are to be uncovered. It is expected that a thorough understanding of the underlying physics of laser-dielectrics interactions will help develop innovative processing technology for traditionally difficult dielectric materials.

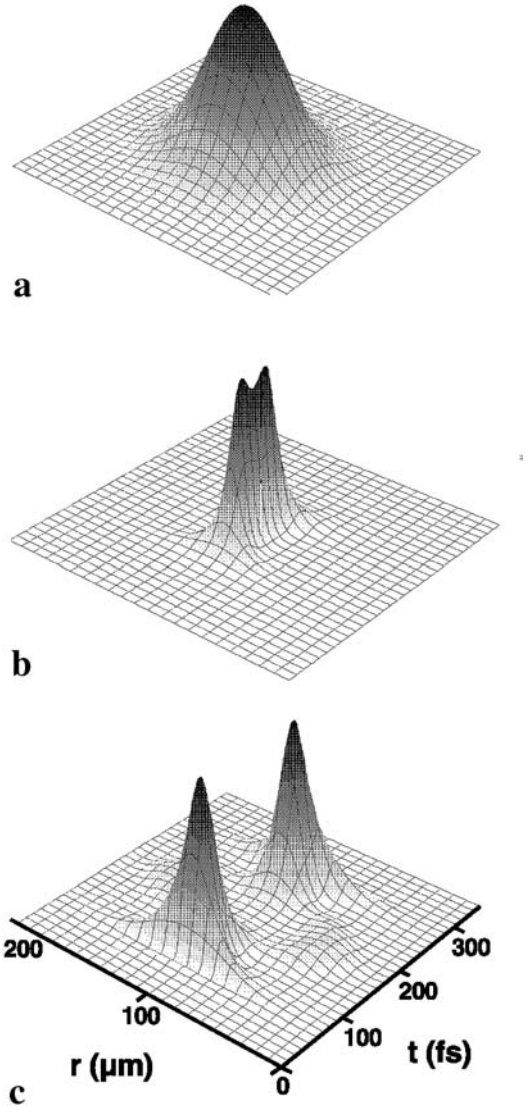

FIGURE 19 Theoretical pulse intensity surface plots of a femtosecond pulse at three different propagation lengths: **a** Input. **b** $z = 2.0$ cm. **c** $z = 3.0$ cm. The pulse intensities were normalized by the peak value [69]

ACKNOWLEDGEMENTS The authors thank S. Diddams, A. Gaeta, B. Ilan, and G. Fibich for sharing their results and providing figures (17, 18, and 19). This work has been supported by the U.S. Department of Energy (DOE) and the French Commissariat à l'Energie Atomique (CEA).

REFERENCES

1 A.H. Zewail: *Femtochemistry: Ultrafast Dynamics of the Chemical Bond* (World Scientific, Singapore 1994)
2 J. Shah: *Ultrafast Spectroscopy of Semiconductors and Semiconductor Nanostructures* (Springer, Berlin Heidelberg New York 1996)
3 C.W. Siders, A. Cavalleri, K. Sokolowski-Tinten, C. Tóth, T. Guo, M. Kammler, M.H. von Hoegen, K.R. Wilson, D. von der Linde, C.P.J. Barty: Science **286**, 1340 (1999)
4 A. Rousse, C. Rischel, S. Foumaux, I. Uschmann, S. Sebban, G. Grillon, Ph. Balcou, E. Förster, J.P. Geindre, P. Audebert, J.C. Gauthier, D. Hulin: Nature **410**, 65 (2001)
5 F. Rossi, T. Kuhn: Rev. Mod. Phys. **74**, 895 (2002)
6 S.K. Sundaram, E. Mazur: Nat. Mater. **1**, 217 (2002)

7 D. Day, M. Gu, A. Smallridge: Opt. Lett. **24**, 948 (1999)
8 H. Ueki, Y. Kawata, S. Kawata: Appl. Opt. **35**, 2456 (1996)
9 E.N. Glezer, M. Milosavljevic, L. Huang, R.J. Finlay, T.-H. Her, J.P. Callan, E. Mazur: Opt. Lett. **21**, 2023 (1996)
10 M. Watanabe, S. Juodkazis, H.-B. Sun, S. Matsuo, H. Misawa: Appl. Phys. Lett. **77**, 13 (2000)
11 H. Sun, Y. Xu, S. Juodkazis, K. Sun, M. Watanabe, S. Matsuo, H. Misawa, J. Nishii: Opt. Lett. **26**, 325 (2001)
12 L.V. Keldysh: Sov. Phys. JETP **20**, 1307 (1965)
13 N.W. Ashcroft, N.D. Mermin: *Solid State Physics* (Saunders, Philadelphia 1976)
14 P.Y. Yu, M. Cardona: *Fundamentals of Semiconductor* (Springer, Berlin Heidelberg New York 1996)
15 M.V. Fischetti, D.J. DiMaria, S.D. Brorson, T.N. Theis, J.R. Kirtley: Phys. Rev. B **31**, 8124 (1985)
16 D. Arnold, E. Cartier: Phys. Rev. B **44**, 10 689 (1991)
17 E. Yablonovitch, N. Bloembergen: Phys. Rev. Lett. **29**, 907 (1972)
18 N. Bloembergen: IEEE J. Quant. Electron. **QE-10**, 375 (1974)
19 B.C. Stuart, M.D. Feit, S. Herman, A.M. Rubenchik, B.W. Shore, M.D. Perry: Phys. Rev. B **53**, 1749 (1996)
20 M. Li, S. Menon, J.P. Nibarger, G.N. Gibson: Phys. Rev. Lett. **82**, 2394 (1999)
21 G. Petite, S. Guizard, P. Martin, F. Quéré: Phys. Rev. Lett. **83**, 5182 (1999)
22 G.L. Yudin, L.N. Gaier, M. Lein, P.L. Knight, P.B. Corkum, M.Y. Ivanov: Laser Phys. **14**, 51 (2004)
23 T. Seideman, M.Y. Ivanov, P.B. Corkum: Phys. Rev. Lett. **75**, 2189 (1995)
24 Y.R. Shen: *The principles of Nonlinear Optics* (Wiley, New York 1984)
25 P.L. Kelley: Phys. Rev. Lett. **15**, 1005 (1965)
26 J.H. Marburger, W.G. Wagner: IEEE J. Quant. Electron. **QE-3**, 415 (1967)
27 K.S. Song, R.T. Williams: *Self-Trapped Excitons* (Springer, Berlin Heidelberg New York 1993)
28 R.F. Haglund, Jr., N. Itoh: In: *Laser Ablation. Principles and Applications*, ed by J.C. Miller (Springer, Berlin Heidelberg New York 1994)
29 M. Ueta, H. Kanzaki, K. Kobayashi, Y. Toyozawa, E. Hanamura (eds.): *Excitonic Processes in Solids* (Springer, Berlin Heidelberg New York 1986)
30 A.N. Vasil'ev, Y. Fang, V.V. Mikhailin: Phys. Rev. B **60**, 5340 (1999)
31 Y. Toyozawa: In: *Relaxation of Elementary Excitations* (Springer, Berlin, Heidelberg, New York 1980)
32 N. Itoh: Adv. Phys. **31**, 491 (1982)
33 A.N. Trukhin: J. Non-Crystal. Solids **149**, 32 (1992)
34 T. Sujiyama, H. Fujiwara, T. Suzuki, K. Tanimura: Phys. Rev. B **54**, 15 109 (1996)
35 E.D. Thoma, H.M. Yochum, R.T. Williams: Phys. Rev. B **56**, 8001 (1997)
36 S. Guizard, P. Martin, G. Petite, P. D'Oliveira, P. Meynadier: J. Phys. Condens. Matter **8**, 1281 (1996)
37 I. Tanimura, T. Tanaka, N. Itoh: Phys. Rev. Lett. **51**, 423 (1983)
38 M. Lenzner: Int. J. Mod. Phys. B **13**, 1559 (1999)
39 A.-C. Tien, S. Backus, H. Kapteyn, M. Murnane, G. Mourou: Phys. Rev. Lett. **82**, 3883 (1999)
40 A. Kaiser, B. Rethfeld, M. Vicanek, G. Simon: Phys. Rev. B **61**, 11 437 (2000)
41 R. Stoian, D. Ashkenasi, A. Rosenfeld, E.E.B. Campbell: Phys. Rev. B **62**, 13 167 (2000)
42 R. Stoian, A. Rosenfeld, D. Ashkenasi, I.V. Hertel, N.M. Bulgakova, E.E.B. Campbell: Phys. Rev. Lett. **88**, 097 603 (2002)
43 Note here that an important energy relaxation mechanism, known as "plasmon losses", has been so far disregarded in the models of laser interaction with dielectrics despite the fact that it is well documented in both theoretical and experimental works on energy losses in dielectrics.
44 X. Mao, S.S. Mao, R.E. Russo: Appl. Phys. Lett. **82**, 697 (2003)
45 C. Iaconis, I.A. Walmsley: Opt. Lett. **23**, 792 (1998)
46 F. Quéré, J. Itatani, G.L. Yudin, P.B. Corkum, Phys. Rev. Lett. **90**, 73 902 (2002)
47 J.P. Geindre, P. Audebert, S. Rebibo, J.-C. Gauthier: Opt. Lett. **26**, 1612 (2001)
48 S.S. Mao, X. Mao, R. Greif, R.E. Russo: Appl. Phys. Lett. **77**, 2464 (2000)
49 P. Martin, S. Guizard, P. Daguzan, G. Petite, P. D'Oliviera, P. Meynadier, M. Perdrix: Phys. Rev. B **55**, 5799 (1997)
50 F. Quéré, S. Guizard, P. Martin: Europhys. Lett. **56**, 138 (2001)
51 K. Tanimura, H. Fujiwara: Proceedings of the 13th ICDIM (Winston-Salem, NC, July 1996). In: "Material Science Forum", vol 239–241, 549, ed by H.G. Mattews, R.T. Williams (Trans Tech., Zurich 1997)
52 R.T. Williams, B.B. Craig, W.L. Faust: Phys. Rev. Lett. **52**, 1709 (1984)
53 T. Shibata, S. Iwai, T. Tokisaki, K. Tanimura, A. Nakamura, N. Itoh: Phys. Rev. B **49**, 13 255 (1994)
54 G.D. Mahan: *Many Particles Physics* (Plenum, New York 1990)
55 P. Daguzan, P. Martin, S. Guizard, G. Petite: Phys. Rev. B **52**, 17 099 (1995)
56 H.J. Kreuzer: *Non-equilibrium Thermodynamics and Its Statistical Foundations* (Clarendon, Oxford 1981)
57 H. Fröhlich: Adv. Phys. **3**, 325 (1954)
58 J. Schilp, T. Kuhn, G. Mahler: Phys. Rev. B **50**, 5435 (1994)
59 H. Haug, S.W. Koch: *Quantum Theory of the Optical and Electronic Properties of Semiconductors* (World Scientific, New York 1993)
60 G. Onida, L. Reining, A. Rubio: Rev. Mod. Phys. **74**, 601 (2002)
61 E. Runge, J.F. Gross: Phys. Rev. Lett. **52**, 997 (1984)
62 A. Braun, G. Korn, X. Liu, D. Du, J. Squier, G. Mourou: Opt. Lett. **20**, 73 (1995)
63 A. Brodeur, O.G. Kosareva, C.Y. Chien, F.A. Ilkov, V.P. Kandidov, S.L. Chin: Opt. Lett. **22**, 304 (1997)
64 B. La Fontaine, F. Vidal, Z. Jiang, C.Y. Chien, D. Comtois, A. Desparois, T.W. Johnston, J.-C. Kieffer, H. Pepin, H.P. Mercure: Phys. Plasmas **6**, 1615 (1999)
65 S. Tzortzakis, L. Sudrie, M. Franco, B. Prade, A. Mysyrowicz, A. Couairon, L. Bergé: Phys. Rev. Lett. **87**, 3902 (2001)
66 S. Henz, J. Herrmann: Phys. Rev. A **59**, 2528 (1999)
67 V.I. Bespalov, V.I. Talanov: JETP Lett. **3**, 307 (1966)
68 G. Fibich, B. Ilan: Phys. D **157**, 112 (2001)
69 S.A. Diddams, H.K. Eaton, A.A. Zozulya, T.S. Clement: IEEE J. Sel. Top. Quant. Electron. **4**, 306 (1998)
70 J.E. Rothenberg: Opt. Lett. **17**, 583 (1992)
71 J. Ranka, R.W. Schirmer, A. Gaeta: Phys. Rev. Lett. **77**, 3783 (1996)
72 J.K. Ranka, A.L. Gaeta: Opt. Lett. **23**, 534 (1998)
73 R.R. Alfano, S.L. Shapiro: Phys. Rev. Lett. **24**, 584 (1970)
74 G.Y. Yang, Y.R. Shen: Opt. Lett. **9**, 510 (1984)
75 A. Brodeur, S.L. Chin: Phys. Rev. Lett. **80**, 4406 (1998)
76 A. Brodeur, S.L. Chin: J. Opt. Soc. Am. B **16**, 637 (1999)
77 A.A Zozulya S.A. Diddams, A.G. van Engen, T.S. Clement: Phys. Rev. Lett. **82**, 1430 (1999)
78 A. L. Gaeta: Phys. Rev. Lett. **84**, 3582 (2000)